AFRL-RZ-WP-TP-2009-2208

ROLLING CONTACT FATIGUE LIFE AND SPALL PROPAGATION CHARACTERISTICS OF AISI M50, M50 NiL, AND AISI 52100, PART I–EXPERIMENTAL RESULTS (PREPRINT)

Lewis Rosado, Nelson H. Forster, Kevin L. Thompson, and 2nd Lt. Jason W. Cooke

Mechanical Systems Branch
Turbine Engine Division

OCTOBER 2009

AIR FORCE RESEARCH LABORATORY
PROPULSION DIRECTORATE
WRIGHT-PATTERSON AIR FORCE BASE, OH 45433-7251
AIR FORCE MATERIEL COMMAND
UNITED STATES AIR FORCE

REPORT DOCUMENTATION PAGE

Form Approved
OMB No. 0704-0188

1. REPORT DATE *(DD-MM-YY)*	2. REPORT TYPE	3. DATES COVERED *(From - To)*
October 2009	Journal Article Preprint	01 May 2006 – 01 May 2008

4. TITLE AND SUBTITLE
ROLLING CONTACT FATIGUE LIFE AND SPALL PROPAGATION CHARACTERISTICS OF AISI M50, M50 NiL, AND AISI 52100, PART I– EXPERIMENTAL RESULTS (PREPRINT)

5a. CONTRACT NUMBER
In-house

5b. GRANT NUMBER

5c. PROGRAM ELEMENT NUMBER
62203F

6. AUTHOR(S)
Lewis Rosado, Nelson H. Forster, Kevin L. Thompson, and 2nd Lt. Jason W. Cooke

5d. PROJECT NUMBER
3048

5e. TASK NUMBER
06

5f. WORK UNIT NUMBER
304806IH

7. PERFORMING ORGANIZATION NAME(S) AND ADDRESS(ES)
Mechanical Systems Branch (AFRL/RZTM)
Turbine Engine Division
Air Force Research Laboratory, Propulsion Directorate
Wright-Patterson Air Force Base, OH 45433-7251
Air Force Materiel Command, United States Air Force

8. PERFORMING ORGANIZATION REPORT NUMBER
AFRL-RZ-WP-TP-2009-2208

9. SPONSORING/MONITORING AGENCY NAME(S) AND ADDRESS(ES)
Air Force Research Laboratory
Propulsion Directorate
Wright-Patterson Air Force Base, OH 45433-7251
Air Force Materiel Command
United States Air Force

10. SPONSORING/MONITORING AGENCY ACRONYM(S)
AFRL/RZTM

11. SPONSORING/MONITORING AGENCY REPORT NUMBER(S)
AFRL-RZ-WP-TP-2009-2208

12. DISTRIBUTION/AVAILABILITY STATEMENT
Approved for public release; distribution unlimited.

13. SUPPLEMENTARY NOTES
Journal article submitted to the Society of Tribologists and Lubrication Engineers.
PAO Case Number: 88ABW-2009-2626, 16 Jun 2009. Paper contains color.

14. ABSTRACT
This paper is the first part of a three-part series which investigates the rolling contact fatigue (RCF) initiation and spall propagation characteristics of three bearing materials, namely AISI 52100, VIM-V AR AISI M50, and VIM-V AR M50NiL steels. Although there is substantial prior work published on the rolling contact fatigue initiation of these materials, little has been published on their spall propagation characteristics after spall initiation. It is recognized that rapid spall growth can lead to catastrophic bearing failure. Hence, understanding the spall growth phase and factors which may cause accelerated growth rates is key to achieving a reliable and robust bearing design. The end goal is to identify control parameters for optimizing bearing materials for improved spall growth resistance. This first part study features the experimental results from 208-size (40 mm bore) angular-contact ball bearings endurance life tested at maximum Hertzian contact stress levels of 3.10 GPa and bearing outer race temperatures up to 131°C. Spall propagation experiments were conducted on new and life tested bearings at 2.10 and 2.4 1 GPa maximum contact stress.

15. SUBJECT TERMS
Rolling element bearings, rolling contact fatigue life, fatigue crack propagation, hybrid ceramic bearings, oil debris monitoring

16. SECURITY CLASSIFICATION OF:			17. LIMITATION OF ABSTRACT:	18. NUMBER OF PAGES	19a. NAME OF RESPONSIBLE PERSON (Monitor)
a. REPORT	b. ABSTRACT	c. THIS PAGE			Garry D. Givan
Unclassified	Unclassified	Unclassified	SAR	54	19b. TELEPHONE NUMBER *(Include Area Code)* N/A

Standard Form 298 (Rev. 8-98)
Prescribed by ANSI Std. Z39-18

Rolling Contact Fatigue Life and Spall Propagation of AISI M50, M50NiL, and AISI 52100, Part I – Experimental Results

Lewis Rosado
Member, STLE
Nelson H. Forster
STLE Fellow
Kevin L. Thompson
2nd Lt. Jason W. Cooke

Propulsion Directorate
Air Force Research Laboratory
Wright-Patterson AFB OH 45433

ABSTRACT

This paper is the first part of a three-part series which investigates the rolling contact fatigue (RCF) initiation and spall propagation characteristics of three bearing materials, namely AISI 52100, VIM-VAR AISI M50, and VIM-VAR M50NiL steels. Although there is substantial prior work published on the rolling contact fatigue initiation of these materials, little has been published on their spall propagation characteristics after spall initiation. It is recognized that rapid spall growth can lead to catastrophic bearing failure. Hence, understanding the spall growth phase and factors which may cause accelerated growth rates is key to achieving a reliable and robust bearing design. The end goal is to identify control parameters for optimizing bearing materials for improved spall growth resistance. This first part study features the experimental results from 208-size (40 mm bore) angular-contact ball bearings endurance life tested at maximum Hertzian

contact stress levels of 3.10 GPa and bearing outer race temperatures up to 131 °C. Spall propagation experiments were conducted on new and life tested bearings at 2.10 and 2.41 GPa maximum contact stress. Spall propagation experiments show that all materials exhibit a rapid or critical spall growth rate after undergoing an initial low-rate spall growth period. The time-to-critical growth rate is dependent on contact stress and was swiftest in AISI 52100 steel. To better understand the underlying physics, driving factors and failure mechanisms, the state of stress is modeled using Finite Element Analysis in Part II and an in-depth microstructural analysis of selected bearings is presented in Part III.

KEYWORDS: rolling element bearings, gas turbine engines, rolling contact fatigue, fatigue crack propagation, hybrid ceramic bearings, oil debris monitoring

INTRODUCTION

The rolling contact fatigue life (RCF) of bearing materials has been extensively studied (1-8). The classical work by Lundberg and Palmgren (L-P) (1-2) is widely accepted as the fundamental method for predicting bearing life. Modifications or life adjustment factors to the L-P life model are currently used as standard practice to account for improvements in bearing material cleanliness and processing, lubrication, presence of subsurface residual stresses, and operating conditions (9-11). Nonetheless, bearing fatigue life, as considered in these studies, has generally been recognized as being the time or stress cycles required for a small spall to develop on the bearing contact surfaces, raceway or rolling elements, as typically depicted in Figure 1. From a practical or

macroscopic viewpoint, this could be considered as the culmination of the initiation phase of contact fatigue and the end of the bearing's useful life, normally labeled as L_n, where n denotes the reliability level desired. Typically n = 10 (90% reliability), though n values of 0.1 or lower are common practice for modern aerospace bearing components where very high reliability and safety is required. It is understood however, that the fatigue initiation process from a classical sense involves nano-scale material changes from accumulated subsurface damage induced by cyclic stress and strain. This in turn may result in localized sites for crack nucleation. Additionally, it is well known that subsurface inhomogeneities such as carbides, non-metallic inclusions and voids could serve as stress concentration sites for crack initiation. Micro-structural changes such as martensitic decay due to rolling contact cyclic loading have also been observed and shown to play a key role in the rolling contact fatigue initiation process (12-15). Hence, significant effort has been undertaken over the past decades in developing cleaner, more homogenous materials with refined microstructures and alloy strengthening resulting in vast improvements in fatigue initiation resistance as seen today with modern bearings. Although a significant body of literature exists on rolling contact fatigue life of bearing materials as described above, very few experimental studies are published on characterizing the spall propagation or spall growth rate, that is, after a spall has initiated and fully developed on the surface (16 - 18). Furthermore, it is of special interest to determine the underlying mechanisms that control rolling contact fatigue spall growth in order to extend the time before a bearing failure progresses from a small spall, as shown in Figure 1, to catastrophic raceway fracture. The effect of maximum Hertzian contact stress and/or subsurface state of stress, material composition and micro-structure, and the

presence of subsurface residual compressive stress fields are factors that intuitively would seem to have an effect on the growth rate of a fatigue spall. Local material properties at the spall edges and front, such as local fracture toughness and yield strength, also seem important in regulating spall growth rate and may change as spall growth progresses.

This paper is the first part of a three-part series which investigates the rolling contact fatigue initiation and spall propagation characteristics of three bearing materials, namely AISI 52100, VIM-VAR AISI M50, and VIM-VAR M50NiL steels. By studying these materials, the effect of microstructure, alloy content, and compressive residual stress on spall growth could possibly be deduced since each material exhibits unique features such as presence of compressive residual stress in M50NiL and lower alloy content in AISI 52100 when compared to AISI M50 and M50NiL. The end goal is to identify control parameters that would allow tailoring future bearing materials for improved spall growth resistance. Part I features the experimental fatigue life and spall propagation results from tests performed on 208-size (40 mm bore) angular-contact ball bearings. To understand the underlying physics, driving factors and failure mechanisms, the state of stress is modeled using Finite Element Analysis in Part II and an in-depth microstructural analysis of selected bearings is presented in Part III.

EXPERIMENTAL

Test Bearing Description and Materials

The inner and outer rings of angular-contact ball bearings of 208-size (40 mm bore) were made from AISI 52100, VIM-VAR AISI M50, and VIM-VAR M50NiL

steels. The AISI M50 and M50NiL raceways had a R_a surface roughness of 25.0 nm and were each fabricated from same material heats respectively to a custom design print to ABEC 5 quality and had split inner rings. Each had eleven 12.7 mm diameter ABMA Grade 10 silicon nitride (Si_3N_4) balls, R_a finish of 6.4 nm and one piece machined silver plated AISI 4340 steel cages, piloted on both sides of the outer ring. The outer ring cage-land shoulders of the M50NiL bearings were titanium nitride (TiN) coated per aerospace standard practice. The AISI 52100 bearings were commercially purchased spindle bearings of ABEC 7 quality which had thirteen 11.1 mm diameter AISI 52100 steel balls (ABMA Grade 10, R_a 25.0 nm finish) and a cotton phenolic retainer, piloted on one side of the outer ring. The raceway R_a surface finish for the AISI 52100 bearings was 25.0 nm.

The basic internal geometries, heat treat condition, and measured surface hardness values for each bearing configuration are given in Table 1. The nominal chemical composition of the alloys studied is given in Table 2. Figure 2 shows a typical residual stress profile for the case carburized M50NiL bearings. The compressive residual stress field ranged from ~ 173MPa near the surface to a maximum of ~ 377 MPa at a depth of 1.25 mm. The case depth for the M50NiL bearings, based on hardness depth profiling to a Rc 58, was approximately 1.25 mm.

Endurance Life Experimental Procedure (Fatigue Initiation)

Bearings were endurance life tested in pairs, with each unfailed bearing being treated as censored or suspension in the Weibull analysis, i.e., “least-of-two” statistical design. Six test heads containing two bearings each were simultaneously operated. The

test rig schematic is shown in Figure 3. Bearings were thrust loaded to a maximum Hertzian contact stress at the inner raceway of 3.10 GPa. No external radial load was applied. Both analysis and post-test visual inspection of bearings showed that the ball-track contact ellipse was confined well within the raceways with no indication of running over the raceway shoulders. Adjustments to the applied load were made to account for differences in number of balls, ball size, and ball material for the AISI 52100 bearings to obtain the same maximum Hertz contact stress as in the hybrid bearings. This resulted in a slight difference in the contact ellipse area between the AISI 52100 bearings and the hybrid configurations, with the contact ellipse being approximately 18 percent smaller in the AISI 52100 bearings. It estimated that the smaller contact conformity in the AISI 52100 bearings results in about 1.0 percent reduction in the Heathcote slip when compared to the hybrid AISI M50 and M50NiL bearings.

Bearing outer race temperature was monitored and controlled at 131 °C and shaft rotational speed was 10,000 rpm. This resulted in 3.95×10^6 stress cycles per hour on the AISI M50 and M50NiL and 4.60×10^6 on the 52100 inner raceways. The number of stress cycles is defined as the relative number of ball pass roll-overs on the inner raceway. Each bearing was jet lubricated with aircraft turbine engine oil conforming to MIL-PRF-7808L military specification (nominally 4.0 cSt at 100 °C) which was re-circulated and supplied at a flow rate of 1.5 L/min. The oil was preheated and supplied to the bearings at approximately 99.0 °C and the oil scavenge temperature was typically 121 °C. The calculated central film thickness and initial lambda ratios for each bearing configuration are listed in Table 3 based on the bearing operating temperature of 131 ºC. The six test heads were arranged in pairs such that two test heads shared a common 20

micron filter and lubrication system (three separate lube systems). Each filter was located on the scavenge side. The oil was purged and the system and filters cleaned after each material test series was completed. Analysis of fatigue wear debris indicated the vast majority of particles generated were over 100 microns in size. Oil samples were drawn for total acid number analysis at marked intervals throughout each test and showed no significant degradation. An accelerometer set at 1.0 g RMS and located on the test rig housing between the two bearings, was used to detect fatigue spall failures and automatically shutdown the motor and all test rig services. The time to failure was recorded and analyzed using a commercially available Weibull statistics computer program. Bearings were run uninterrupted until failure or after having reached a nominal suspension time of 3,000 hours (~ 11.9×10^9 inner race stress cycles). However, one pair each of AISI M50 and M50NiL bearings were allowed to run to approximately 5,000 hours (19.7×10^9 inner race stress cycles). A total of nine AISI 52100 bearings and twelve each AISI M50 and M50NiL were life tested. The test order sequence was AISI 52100 bearings first, followed by M50NiL and lastly the AISI M50 bearings.

Spall Propagation Experimental Procedure

Spall propagation experiments were conducted on two separate test heads of the same design as those used for life testing, each containing a slave bearing and a test bearing. The oil flow and rotational speed were the same as the endurance life experiments. The measured bearing outer race temperature was 110° C. Two populations of bearings were investigated; new bearings with no accumulated stress cycles and selected bearings from endurance life tests previously described. Spall propagation

experiments on new pristine bearings were performed at 2.10 GPa and 2.41 GPa maximum contact stress. The new bearings were initially indented with four Rockwell hardness indents with a 150 kg load across the inner raceway in order to induce the initial fatigue spall for propagation. The spall initiation of indented bearings was performed at 2.65 GPa maximum Hertz stress until the vibration exceeded the accelerometer's 1.0 g threshold indicating the formation of a small spall as shown in Figure 4. Initial spalls were typically between 1 to 2 mm in size. The bearings were then each photographically documented and reinstalled for spall propagation. Five replicate bearing samples of each material were run at each stress condition for a total 30 experiments on new bearings.

Selected bearings from the endurance life tests previously described were also spall propagated in an attempt to study the effect of accumulated stress cycles. Spall propagation on these bearings was performed at 2.41 GPa. The endurance life tested bearings selected for propagation are listed in Table 4 with the number of accumulated cycles prior to propagation and whether propagation was performed from natural spalls or indents. Since unfailed suspended bearings from life tests were also propagated, these were similarly indented and initiated as previously described to induce the initial fatigue spall. Bearings with natural spalls from life tests were directly propagated with no pre-conditioning.

Spall growth rate was monitored using an in-line oil debris monitor (ODM) mounted on the oil scavenge line as first described by Muir and Howe (19). The ODM particle release count and mass loss (mg) were plotted as a function of time and number of inner raceway stress cycles. Spalls were propagated until a nominal mass loss of at least 100 mg was achieved, corresponding to a spall about 50 mm in length. The inner

raceways were weighed prior to and after propagation experiments in order to obtain improved fidelity of the mass loss values given by the ODM. In order to eliminate any bias from the indents during the initial spall growth period, ODM data is reported after spalls had reached steady growth or approximately 10 mg of mass loss. The time and number of stress cycles for spalls to grow from 10 mg to 100 mg mass loss was monitored and plotted. Each post tested bearing was photographically documented and detailed microstructural analysis was performed on selected bearings from both groups. These results are reported in Part III (20).

RESULTS AND DISCUSSION

Endurance Fatigue Life Experimental Results

Figure 5 shows the Weibull plot from fatigue initiation life tests. Only one fatigue failure was obtained on AISI M50, with the remaining bearings all reaching the preset suspension time during test and hence being treated as such in the analysis. This increases the uncertainty in the Weibull results for AISI M50. Figure 6 shows a typical fatigue spall for AISI 52100. Spalls for AISI M50 and M50NiL were very similar to that shown in Figure 6. Results show that AISI M50 and M50NiL hybrid bearings exhibit remarkable fatigue initiation resistance over all-metal AISI 52100. However, results suggest that AISI M50 has superior fatigue life over M50NiL, which is inconsistent with previous studies (21 - 23). It is well known that case carburized M50NiL provides superior fatigue life over AISI M50, mostly due to its high residual compressive stress and fine microstructure. Upon closer examination of the bearings, it was discovered that the TiN coating from the M50NiL cage-land surface was delaminating and causing

raceway surface damage as shown in Figures 7 and 8. It is believed that indentations caused by the hard TiN particles served as stress concentration sites for crack initiation and eventual spall formation, undermining overall fatigue life performance of M50NiL. Despite this, M50NiL exhibited an L_{10} of 3.1 billion stress cycles compared to 510 million for AISI 52100. The use of silicon nitride rolling elements is also believed to contribute to the observed improvement over AISI 52100 since it's known that hybrid ceramic bearings offer fatigue life benefits over all-metal bearings.

Theoretical or calculated fatigue lives with appropriate life factors are given in Table 5 for each bearing following the procedures delineated in references (9) and (11). For comparison, experimental L_{10} lives are also shown in Table 5. Relatively good correlation was obtained between calculated and experimental lives for the AISI 52100 bearings. However, poor correlation was obtained on the AISI M50 bearings, with experimental life far exceeding the predicted value. Due to the TiN contamination issue previously described with the M50NiL bearings, the experimental life was significantly less than the predicted value. It should be noted that the life factors used for AISI M50 and M50NiL do not account for the Si_3N_4 ball material used in the experiments. However, it is believed that the hybrid material pair alone could not account for the disparity observed with AISI M50. Further experimental studies should be undertaken to quantify life factors for modern Si_3N_4 ceramic balls and modern VIM-VAR AISI M50 and M50NiL bearings given that the life factors used here were based on data generated during the 1970-80 timeframe. Several selected bearings from life endurance tests, listed in Table 4, were chosen for spall propagation experiments as reported in the next section.

Spall Propagation Experimental Results

Figures 9 and 10 show the spall propagation trend plots for “new” indented AISI 52100, AISI M50, and M50NiL bearings at 2.10 and 2.41 GPa contact stress, respectively. Figure 11 depicts the effect of maximum Hertz contact stress on spall growth of AISI 52100. The mean number of stress cycles for spalls to grow from 10 mg mass loss to 100 mg for new indented bearings is summarized in Figure 12. A typical spall after reaching 100 mg mass loss is shown in Figure 13. It is evident from the spall growth trend curves that all materials typically exhibit an initial low-rate spall growth region followed by rapid critical growth or “knee” in the curve. This was generally observed at both contact stresses and on all materials studied, suggesting a mechanism inherent to rolling contact fatigue spall growth. It is of special interest to understand what causes spalls to reach critical growth since this could provide insight into possible optimization of materials for spall growth resistance. Similar characteristics are readily found in the literature for materials undergoing classical fatigue crack growth, such as in rotating bending, axial loading and as described in fracture mechanics theory (24 - 26). Though the driving factors here may differ from classical fatigue growth due to the complex dynamic and tribological conditions associated with lubricated Hertzian rolling contact fatigue and unique subsurface cyclic stress fields not present in conventional structural applications. Kotzalas and Harris (18) similarly observed two distinct spall growth regions in AISI 52100 steel balls using a single-ball / v-ring test rig. They noted significant and rapidly increasing dynamic or vibratory loads during the fast spall growth region and concluded this to have a major effect in limiting useful bearing life. Interestingly, spall growth model predictions for a rolling contact by Xu and Sadeghi (27)

and Raje et al. (28) also show comparable trends. These studies are based on damage mechanics and discrete material models. Xu and Sadeghi in particular attribute the predicted spall initiation and propagation to the accumulated cyclic plastic strain within the loaded material layer.

As previously mentioned, the spall growth characteristics observed in the present study may be best described through fracture mechanics, where the primary crack propagation driving force is the stress intensity factor (SIF) at subsurface crack tips, in this case beneath the spall front. From a simplistic viewpoint, crack growth occurs when the change in SIF or ΔK exceeds the materials threshold ΔK_{th} value leading to stable growth as observed during the initial low-rate region, analogous to the Paris region described in fracture mechanics. Critical crack growth ensues as the ΔK approaches and exceeds the materials critical ΔK or fracture toughness K_{Ic}. Although the fracture mechanics approach may not exclusively describe the macroscopic spall growth studied here due to likely presence of numerous networks of subsurface cracks, it does provide insight as to possible mechanisms as will be discussed shortly. It is noteworthy that the fracture mechanics approach has been extensively used to model RCF initiation and propagation in rolling contacts in general (29 - 33), though there is some disagreement as to the dominant crack propagation mode. Also, the accumulation of surface and subsurface damage, large scale plasticity effects, and material weakening caused by stress and strain induced microstructural changes also need to be considered. Some of these aspects are studied in more depth by Arakere et al. in Part II (34) and Forster et al. in Part III (20).

Focusing on “new” indented bearings, results indicate that spalls propagate faster in AISI 52100 than in AISI M50 and M50NiL and that contact stress has a significant effect on spall growth rates. Figure 12 shows that the difference in mean spall propagation times between AISI 52100 and AISI M50 and AISI 52100 and M50NiL are statistically significant and it generally takes one to two orders of magnitude more stress cycles for spalls in AISI M50 and M50NiL to reach critical levels when compared to AISI 52100. It should be noted that the geometrical and material differences between the all-metal / phenolic cage AISI 52100 and hybrid ceramic / steel cage AISI M50 and M50NiL bearings would intuitively result in different bearing dynamics that may in turn affect spall propagation rates. Thus caution should be taken when comparing the spall growth characteristics of AISI 52100 with AISI M50 and M50NiL. Interestingly, spalls tended to grow slower in AISI M50 than in M50NiL, though the difference was not significant at the lower 2.10 GPa contact stress. The M50NiL bearings were examined for any evidence of TiN delamination as seen on bearings from endurance life experiments that would explain this result, but coatings appeared intact in all the spall propagated bearings. Note that endurance life tested bearings were run for much longer times than those in spall propagation experiments. *The observation on M50NiL may be explained considering that spall growth occurs within the confines of the brittle carburized case.* Thus, local case material properties would dominate crack growth. This has been postulated before (35 - 37) and experimental data on the case fracture properties of M50NiL show that ΔK_{th} and K_{Ic} values are significantly lower than in the core as shown in Table 6. Averbach et al. (35) reported K_{Ic} values for M50NiL through carburized cases lower than through hardened AISI M50. Fracture toughness properties for the M50NiL

carburized case are actually closer to AISI 52100 as shown in Table 6. This suggests the residual compressive stress in M50NiL helped retard crack propagation, with a resulting net effect of spall growth similar to AISI M50. It is believed the combined effect of low fracture toughness in the M50NiL carburized case and its high residual compressive stress results in spall growth resistance better than AISI 52100 but not substantially different than AISI M50. Note that these results are for "new" indented bearings with no previous accumulated stress cycle history.

Results given in Figure 12 also show there is significantly more variance at the lower 2.10 GPa contact stress, particularly with AISI M50 and M50NiL. The variance diminished substantially for both materials at the higher 2.41 GPa stress suggesting a shift from a stochastic process to a more deterministic one at higher stress. At lower stress, it appears that spall propagation in AISI M50 and M50NiL retains the probabilistic character typically observed during fatigue initiation and generally described with Weibull statistics. As contact stress is increased, it is unclear what causes a shift towards a more deterministic behavior, though possibilities include a more direct correlation with deterministic fracture mechanics properties due to the higher SIF. On the other hand, results on AISI 52100 were quite repeatable at both stresses, suggesting the fracture response in AISI 52100 follows a more deterministic process at the conditions studied here. Tomar and Zhou (39) conclude that microstructures less prone to fracture, such as in AISI M50 and M50NiL in this case, show higher variation in fracture response when compared to ones that offer least resistance to crack propagation. Also, the standard deviation of predicted time to failure of structural components generally follows an

inverse relationship to the applied excitation stress amplitude (40), which is consistent with the observations presented here.

As previously stated, a limited number of bearings from endurance life experiments were spall propagated per Table 4 in an attempt to study the effect of accumulated stress cycles on spall growth. This represents a more realistic scenario since bearings in actual operation may undergo billions of stress cycles before initial spall formation and eventual propagation. Note from Table 4 that both life tested AISI M50 bearings had accumulated approximately 17.0 billion stress cycles during life tests, prior to propagating the spalls. The M50NiL bearings also had a high number of accumulated stress cycles, which ranged from 5.7 to 19.6 billion. Due to its lower fatigue life, the two AISI 52100 bearings had fewer cycles prior to propagation, 25.0 and 603.0 million cycles. Spalls were propagated on these at 2.41 GPa contact stress. Results are presented in Figures 14 and 15. Similar to new indented bearings, spall growth is generally characterized by two distinct regions, sub-critical followed by critical growth. However, results indicate there is a difference between spalls grown on ‘new” indented AISI M50 bearings at 2.41 GPa and those grown on life tested AISI M50, with spalls propagating faster on life endurance bearings (Figure 15). The high number of accumulated stress cycles on AISI M50 probably resulted in subsurface damage which weakened the material resulting in higher spall propagation rate. If confirmed, this result is of practical importance in that it implies a spall will tend to grow faster on a high cycle AISI M50 bearing than on a bearing with fewer accumulated cycles. Interestingly, there was no significant difference observed for life tested AISI 52100 and M50NiL bearings when compared to new indented ones. The result for M50NiL is intriguing in that despite that

the bearings had a significant amount of accumulated cycles, spall propagation rate was about the same as new indented bearings. No clear explanation is given here, though residual compressive stress and microstructural differences are suspect. A more stable microstructure, less prone to stress and strain induced changes may also explain the result for M50NiL. It should be noted that the results are based on a small number of samples and hence, caution should be taken when interpreting the results. Further experimental work and analysis is required to confirm the findings. Towards this end, microstructural analysis of selected bearings is presented in Part III (20).

SUMMARY OF RESULTS

Rolling contact fatigue life endurance and spall propagation experiments were conducted on 208-size angular-contact ball bearings made of three materials, namely AISI 52100, AISI M50, and M50NiL. Fatigue life results show that AISI M50 and M50NiL hybrid bearings outperform AISI 52100 bearings as expected. However, M50NiL bearings exhibited lower fatigue life than AISI M50, contrary to previous studies. Closer examination of M50NiL bearings revealed that the TiN coating on the cage-land shoulder was shedding, causing secondary damage and hard particle indentation of the M50NiL raceway surfaces, undermining its fatigue life. Good correlation was obtained between experimental and calculated fatigue lives for AISI 52100. However, experimental fatigue lives far exceed the calculated L_{10} life for AISI M50 bearings, suggesting improvements to life adjustment factors should be made to account for modern bearing technology.

Spall propagation experiments on ‘new” indented and endurance life tested bearings revealed two general spall growth regions, an initial low-rate region followed by critical growth. This characteristic was observed in all materials and test conditions studied, suggesting an attribute inherent to macroscopic rolling contact fatigue spall growth. The behavior was discussed as being coupled to material fracture response as described by classical fracture mechanics. Spall growth rates in “new” indented AISI M50 and M50NiL bearings were significantly lower than in AISI 52100 bearings, believed to be a result of the higher fracture toughness in AISI M50, the high residual compressive stress in M50NiL and more stable microstructures of both of these materials. However, firm conclusions could not be drawn due to differences in bearing geometry and ball and cage materials used in the AISI 52100 bearings. Future studies should be undertaken to investigate the effect of ball-train mass on spall growth rates. Interestingly, comparable spall growth rates were observed in AISI M50 and M50NiL bearings, particularly at the lower 2.10 GPa contact stress. At the higher 2.41 GPa contact stress, spalls in new indented AISI M50 bearings grew consistently slower than in M50NiL, which was unexpected. The behavior was discussed as being attributed to the low fracture toughness properties of the brittle, carburized case in M50NiL.

The effect of accumulated stress cycles on spall growth was investigated by propagating spalls on a limited number of bearings from previous fatigue life experiments. Preliminary results showed that spalls propagated faster in AISI M50 bearings with accumulated cycles than in bearings with no prior cycle history, suggesting spall growth rate in AISI M50 may be dependent on the extent of accumulated damage. The results on M50NiL were interesting in that no difference was observed in spall

growth rates between high cycle bearings and new indented ones. It is believed the high residual compressive stress and microstructural differences may play a role in the resulting spall growth behavior observed on life tested M50NiL bearings. In closing, the macroscopic spall propagation response of bearing materials appears to involve complex processes that depend on the balance of near surface material fracture properties, presence of residual compressive stress fields, alloy composition, and extent of accumulated damage. Additional experimental data and analysis are clearly needed to draw firm conclusions.

ACKNOWLEDGMENTS

The authors wish to express their gratitude to Dr. Elizabeth Cooke and Mr. John Imundo of The Timken Company for providing the M50NiL bearings and microstructural and case profile results. Also to Mr. Hitesh Trivedi of UES, Inc. for conducting the fatigue life rig tests, data acquisition, and photomicrographs and Mr. Chris Klenke of AFRL for the SEM micrographs. This work was funded by the Propulsion Directorate, Air Force Research Laboratory.

REFERENCES

1. Lundberg, G. and Palmgren, A. (1947), "Dynamic Capacity of Rolling Bearings," *Acta Polytech. Mech. Engr. Ser.* Vol 1, No.3.
2. Lundberg, G. and Palmgren, A. (1952), "Dynamic Capacity of Roller Bearings," *Acta Polytech. Mech. Engr. Ser.* Vol 2, No.4.
3. Tallian, T. (1962), "Weibull Distribution of Rolling Contact Fatigue Life and Deviations Therefrom," *ASLE Trans*. **5** (1),.
4. Anderson, W. J. (1987), Bearing Fatigue Life Prediction," National Bureau of Standards, No. 43NANB716211.
5. Jones, A. B. (1952), "The Life of High-Speed Ball Bearings," *ASME Trans.*, **74** (5).
6. Parker, R. J. and Zaretsky, E. V. (1978), "Rolling Element Fatigue Life of AISI M-50 and 18-4-1 Balls," NASA TP-1202.
7. Zaretsky, E.V. and Anderson, W. J. (1966), "Material Properties and Processing Variables and Their Effect on Rolling-Element Fatigue," NASA TM X-52227.
8. Bamberger, E. N., Zaretsky, E. V., and Signer, H. (1976), "Endurance and Failure Characteristics of Main-Shaft Jet Engine Bearings at 3x106 DN," *J. of Lubr. Tech.*, **98** (4).
9. Bamberger, E. N., Harris, T. A., Kacmarsky, W. M., Moyer, C. A., Parker, R. J., Sherlock, J. J., and Zaretsky, E. V. (1971), "Life Adjustment Factors for Ball and Roller Bearings, An Engineering Design Guide," ASME, N.Y.

10. Ioannides, E. and Harris, T. A. (1985), "A New Fatigue Life Model for Rolling Bearings," *J. of Trib.*, **107**.

11. Zaretsky, E. V. (1999), "STLE Life Factors for Rolling Bearings," 2nd Ed., STLE Publication SP-34.

12. Jones, A.B. (1946), Metallographic Observations of Ball Bearing Fatigue Phenomena," *Proc. ASTM*, **46**.

13. Martin, J. A., Borgese, S.F., and Eberhardt, A.D. (1966), "Microstructural Alterations of Rolling Bearing Steel Undergoing Cyclic Stressing," *J. of Basic Engrg, Trans. Of ASME*.

14. Swahn, P. C. Becker, and Vingsbo, O. (1976), "Martensite Decay During Rolling Contact Fatigue in Ball Bearings," *Metallurgical Trans A*, 7A.

15. Voskamp, A. P. and Mittemiejer, E. J. (1997), "The Effect of The Changing Microstructure on The Fatigue Behaviour During Cyclic Rolling Contact Loading," *Z. Metallkd*, **88** (4).

16. Hoeprich, M. R. (1992), "Rolling Element Bearing Fatigue Damage Propagation," *ASME J. of Trib.*, **114**, pp. 328-333.

17. Li, Y., Billington, S., Zhang, C., Kurfess, T., Danyluk, S., and Liang, S. (1999), "Dynamic Prognostic Prediction of Defect Propagation on Rolling Element Bearings," *STLE Trib. Trans.*, **42** (2), pp. 385-392.

18. Kotzalas, M. N. and Harris, T. A. (2001), "Fatigue Failure Progression in Ball Bearings," *J. of Trib., Trans. Of the ASME*, **123**, pp. 238-242.

19. Muir, D. and Howe, B. (1996), “In-Line Oil Debris Monitor (ODM) for the Advanced Tactical Fighter Engine,” SAE Technical Paper Series 961308, Aerospace Atlantic Conference, Dayton OH.

20. Forster, N. H., Ogden, W. P., Trivedi, H. K., and Rosado, L., “On the Rolling Contact Fatigue Life and Spall Propagation Characteristics of M50, M50NiL and 52100 Bearing Materials, Part III – Metallurgical Examination,” In print Trib. Trans.

21. Averbach, B. L., Van Pelt, S. G., Pearson, P. K., and Bamberger, E. N. (1991), “Surface-Initiated Spalling Fatigue in M-50 and M-50NiL Bearings,” *Lubr. Eng*., **47**, 10, pp. 837-843.

22. Boehmer, H. J., Ebert, F. J., and Trojhan, W. (1992), “M50NiL Bearing Material – Heat Treatment, Material Properties and Performance in Comparison with M50 and RBD,” *Lubr. Eng*., **48**, 1, pp. 28-35.

23. Harris, T. A., Skiller, J., and Spitzer, R. F. (1992), “On the Fatigue Life of M50NiL Rolling Bearings,” *STLE Trib. Trans*., **35,** 4, pp. 731-737.

24. Akiniwa, Y., Miyamoto, N., Tsuru, H., and Tanaka, K. (2006), “Notch Effect on Fatigue Strength Reduction of Bearing Steel in the Very High Cycle Regime,” *Intl. J. of Fatigue*, **28**, pp. 1555 – 1565.

25. Mohanty, J.R., Verma, B.B., and Ray, P.K. (2009), “Prediction of Fatigue Crack Growth and Residual Life Using an Exponential Model: Part I (Constant Amplitude Loading),” *Intl. J. of Fatigue*, **31**, pp. 418-424.

26. Anderson, T. L. (1995), “Fracture Mechanics: Fundamentals And Applications, 2nd Ed., CRC Press Inc., Boca Raton, FL.

27. Xu, G. and Sadeghi, F. (1996), "Spall Initiation and Propagation Due to Debris Denting," *Wear*, **201**, pp. 106-116.

28. Raje, N., Slack, T., and Sadeghi, F. (2009), "A Discrete Damage Mechanics Model for High Cycle Fatigue in Polycrystalline Materials Subject to Rolling Contact," *Intl. J. of Fatigue*, **31**, pp. 346-360.

29. Keer, L. M. and Bryant, M. D. (1983), "A Pitting Model for Rolling Contact Fatigue," *Trans ASME J. of Lubr. Engr. Tech.*, **105**, pp. 198-205.

30. Datsyshyn, O. P. and Panasyuk, V. V. (2001), "Pitting of the Rolling Bodies Contact Surface," *Wear*, **251**, pp. 1347-1355.

31. Goshima, T., Ishihara, S., Shimizu, M., Yoshida, H., and Tsuchida, Y. (2003), "Surface Crack Growth Path and Fatigue Life Predictions Due to Repeated Rolling / Sliding Contact," *JSME Intl. J. A*, **46,** 4, pp. 582-589.

32. Ekberg, A. and Kabo, E. (2005), "Fatigue of Railway Wheels and Rails Under Rolling Contact and Thermal Loading – An Overview," *Wear*, **258**, pp. 1288-1300.

33. Ringsberg, J. W. (2005), "Shear Mode Growth of Short Surface-breaking RCF Cracks," *Wear*, **258**, pp. 955-963.

34. Arakere, N. K., Branch, N., Levesque, G., Svendsen, V., and Forster, N. H., "On the Rolling Contact Fatigue Life and Spall Propagation Characteristics of M50, M50NiL and 52100 Bearing Materials, Part II – Stress Modeling," In print Trib. Trans.

35. Averbach, B. L., Lou, B., Pearson, P. K., Fairchild, R. E., and Bamberger, E. N. (1985), "Fatigue Crack Propagation in Carburized High Alloy Bearing Steels," *Met. Trans. A*, **16A**, pp. 1253-1265.

36. Fu, Y. Q., Gu, Y., Jing, X., Hu, M., and Bingzhe, L. (1995), "New Method to Evaluate Fracture Toughness of Case-Hardened Steel," *Intl. J. of Fracture*, **71**, pp. R71-R76.

37. Fu, Y. Q., Gu, Y. W., Batchelor, A. W., and Zhou, W. (1998), "Investigation of Fracture Toughness of Deep Carburized M50NiL Steel Under Different Tempering Temperatures," *Matl. Science and Tech.*, **14**, pp. 461-465.

38. Beswick, J. M. (1989), "Fracture and Fatigue Crack Propagation Properties of Hardened 52100 Steel," *Met. Trans. A*, **20A**, pp. 1961-1973.

39. Tomar, V. and Zhou, M. (2005), "Deterministic and Stochastic Analyses of Fracture Processes in a Brittle Microstructure System," *Engr. Fracture Mechanics*, **72**, pp. 1920-1941.

40. Ray, A. and Patankar, R. (1999), "A Stochastic Model of Fatigue Crack Propagation Under Variable-amplitude Loading," *Engr. Fracture Mechanics*, **62**, pp. 477-493.

41. Hamrock, B.J. and Dowson, D., (1976), "Isothermal Elastohydrodynamic Lubrication of Point Contacts, Part II — Ellipticity Parameter Results.," *Trans. ASME, J. Lubrication Tech.*, **98**, pp. 375–383.

LIST OF TABLES AND FIGURES

List of Tables

List of Figures

TABLES

Raceway Material	Ball Material	Ball Diam., mm	No. Balls	Pitch Diam., mm	Initial Contact Angle, deg	Raceway Heat Treat Condition	Avg. Raceway Surface Hardness, HR_c
AISI 52100 Air melt/ vacuum degassed	52100	11.1	13	66.04	15	through hardened, tempered at 200 ºC	62.2
AISI VIM-VAR M50	Si_3N_4	12.7	11	60.25	22	through hardened, tempered at 540 ºC	64.5
VIM-VAR M50NiL	Si_3N_4	12.7	11	60.25	22	case carburized, tempered at 525 ºC	64.5

Table 1. 208-size (40 mm bore) angular contact bearing geometry, heat treat condition and measured surface hardness

Material	Wt % Primary Alloying Elements					
	C	Cr	Ni	V	Mo	Reference
AISI 52100	1.04	1.45	-	-	-	AMS 6440L
AISI VIM-VAR M50	0.80	4.00	0.10	1.00	4.25	AMS 6491A
VIM-VAR M50NiL	0.13	4.00	3.40	1.23	4.25	AMS 6278

Table 2. Nominal wt. % of primary alloying elements of bearing steels

Raceway Material	**Central film thickness h_{min}*, nm**	**Composite R_a surface roughness $\sigma = \sqrt{(\sigma_{ball}^2 + \sigma_{raceway}^2)}$, nm**	**Lambda, $\lambda = h_{min} / \sigma$**
AISI 52100	88.4	35.3	2.5
AISI VIM-VAR M50	93.0	25.7	3.6
VIM-VAR M50NiL	93.0	25.7	3.6

* From (41)

Table 3. Theoretical central film thickness and lambda ratios for endurance life tested bearings

Raceway Material	Bearing Test No.	RCF Life at 3.10 GPa (Hours / Stress cycles x 10^6)
AISI 52100	221B	Spall 131 / 603
AISI 52100	206B	Spall 5.4 / 24.8
AISI M50	216	Suspension 4,267/ 16,855
AISI M50	215	Suspension 4,267/ 16,855
M50NiL	043B	Spall 1,436 / 5,672
M50NiL	046B	Suspension 4,959 / 19,588
M50NiL	045B	Suspension 4,959 / 19,588

Table 4. Bearings propagated from RCF life experiments showing time and number of accumulated stress cycles prior to spall propagation. Natural spalls were propagated with no preconditioning, suspended bearings were propagated from indents.

Bearing Material	Lundberg-Palmgren Basic L_{10} Life (hrs)	Life Factor, a_2 Materials and Processing	Life Factor, a_3 Operating Conditions	STLE Adjusted L_{10A} Life (hrs)	Experimental L_{10} Life (hrs)
CVD AISI 52100 all-metal	11.2	2.04	2.39	54.8	32.8
VIM-VAR AISI M50 / Si_3N_4 balls	30.3	5.46	3.57	589.6	4,202
VIM-VAR M50-NIL / Si_3N_4 balls	30.3	10.92	3.57	1,179	772

$L_{10A} = L_{10}(a_1)(a_2)$

Table 5. Calculated fatigue lives, life adjustments factors, and experimental fatigue life for 208-size angular contact ball bearings. Life factors obtained from (9) and (11).

Material	**ΔK_{th} (MPa · m ^{½})**	**Ref.**	**K_{Ic} (MPa · m ^{½})**	**Ref.**
Hardened AISI 52100	~ 3.9	(38)	~17.5	(38)
AISI M50	4.8	-	23.0	(35)
M50NiL case	2.8	-	16.0	(35)
M50NiL core	7.4	-	50.0	(35)

Table 6. Fracture properties for through hardened and case carburized bearing steels.

FIGURES

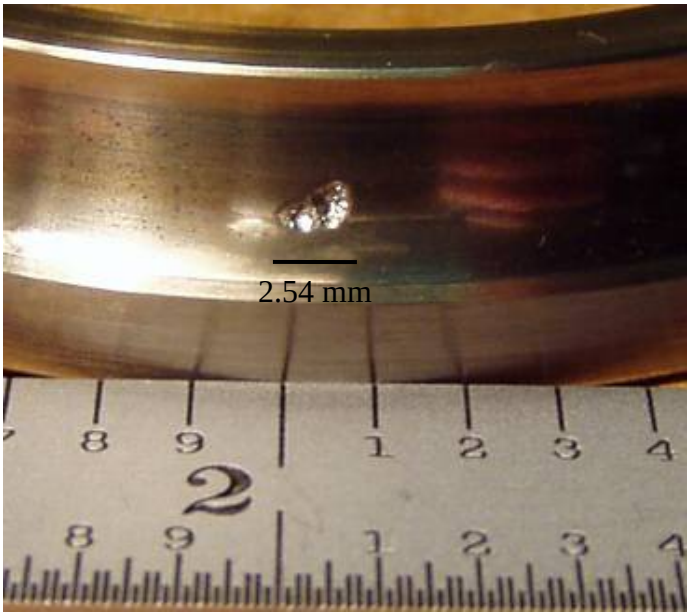

Figure 1. Typical fatigue spall

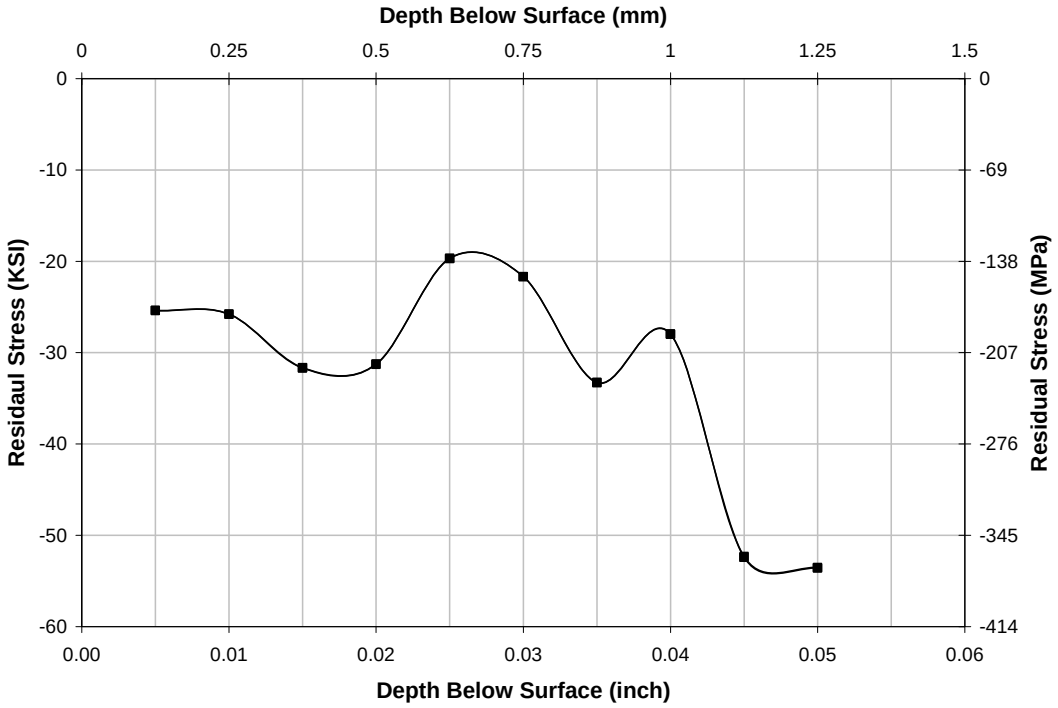

Figure 2. Residual stress profile of case-carburized M50NiL

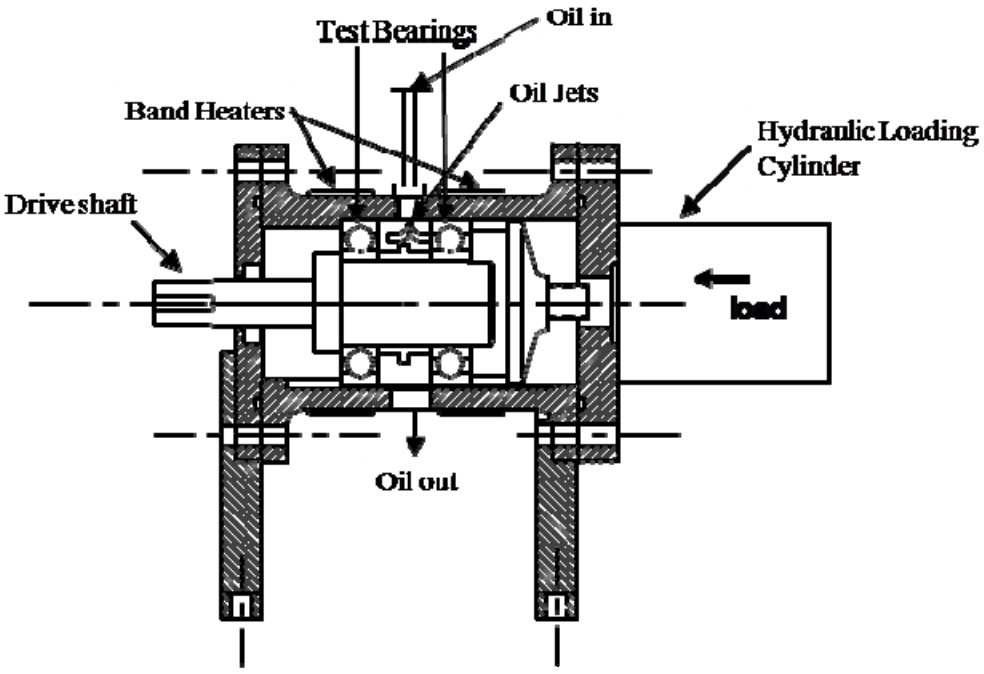

Figure 3. Bearing fatigue and spall propagation test rig schematic

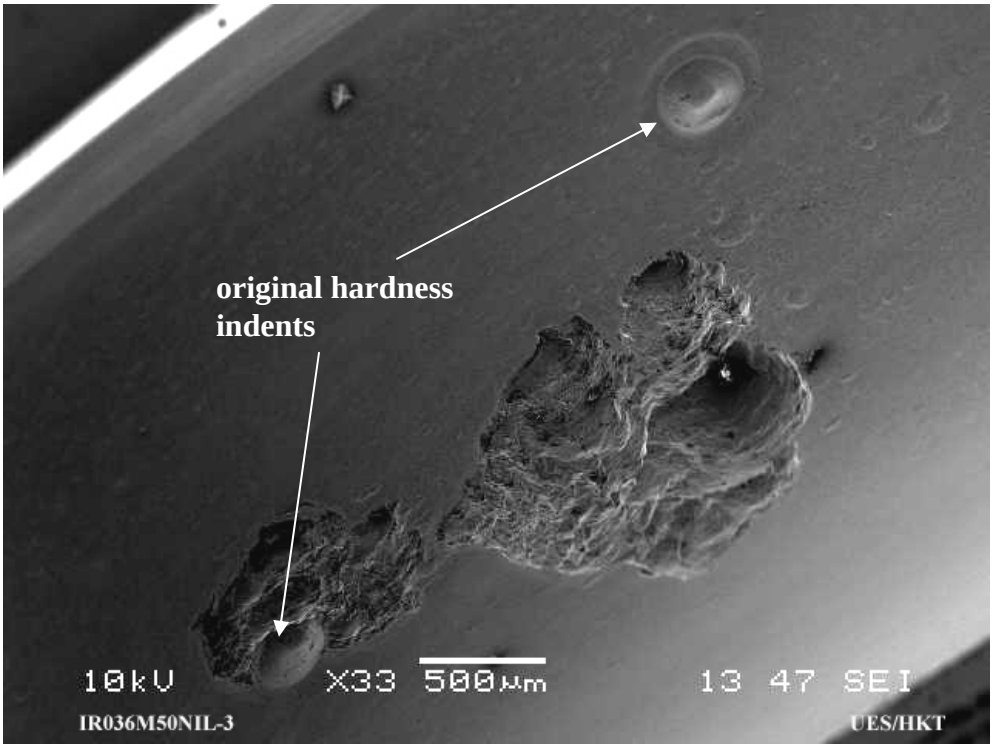

Figure 4. SEM micrograph showing initial spall developing from hardness indents on M50NiL bearing.

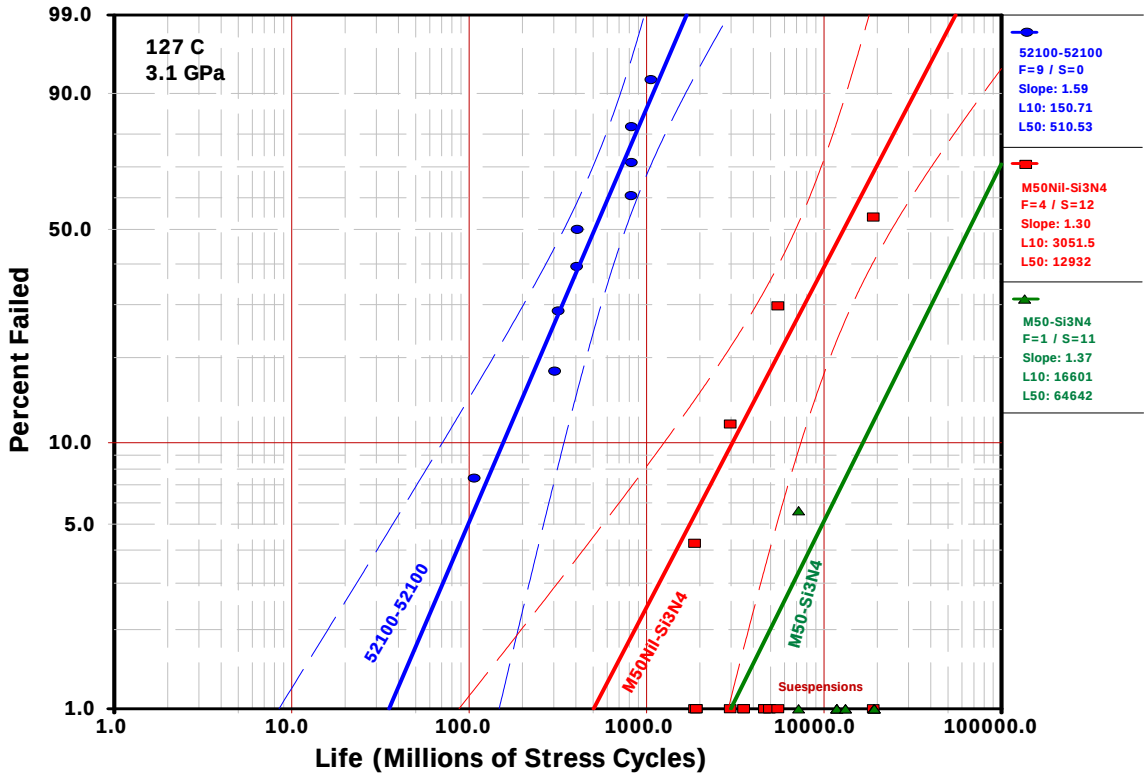

Figure 5. Weibull RCF life results showing fatigue initiation life of AISI 52100, AISI M50 and M50NiL bearings. 90% confidence bands shown for AISI 52100 and M50NiL.

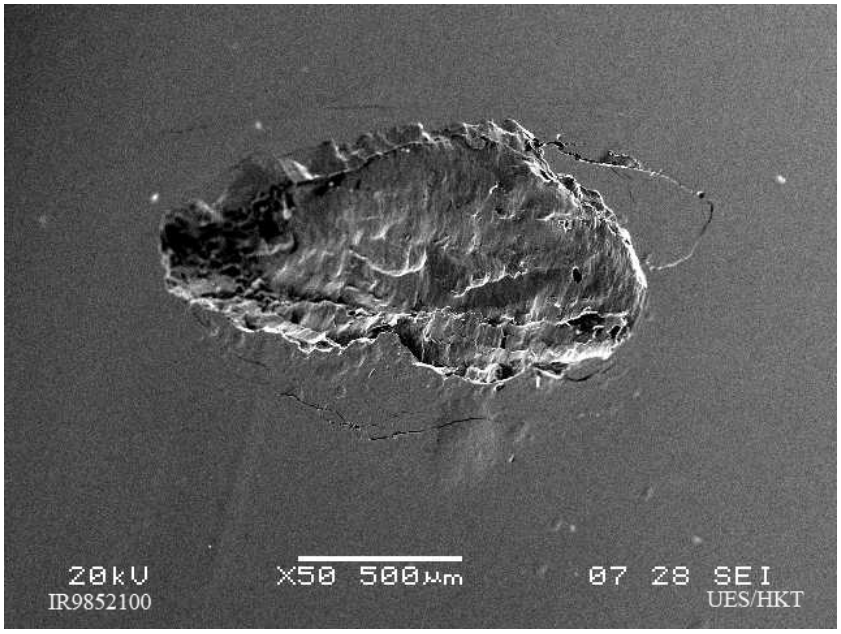

Figure 6. Typical fatigue spall on 52100 from endurance life experiments.

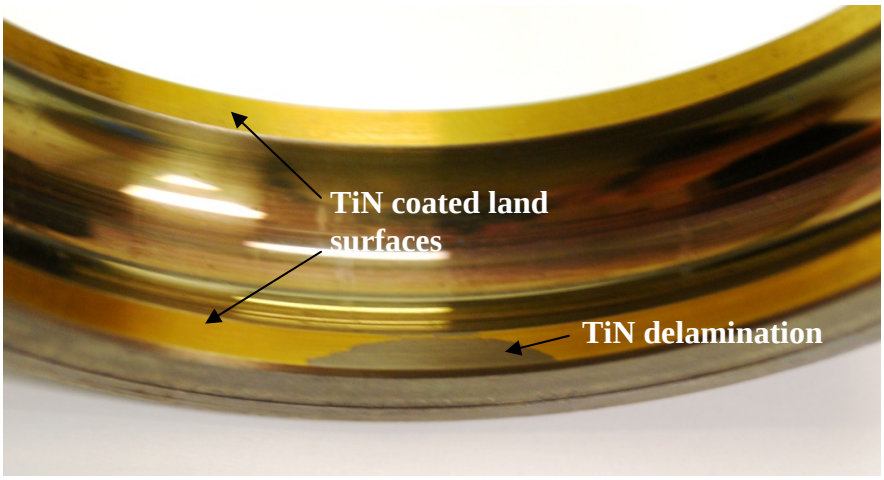

Figure 7. Evidence of TiN coating delamination on M50NiL bearing outer race cage-land surface.

.

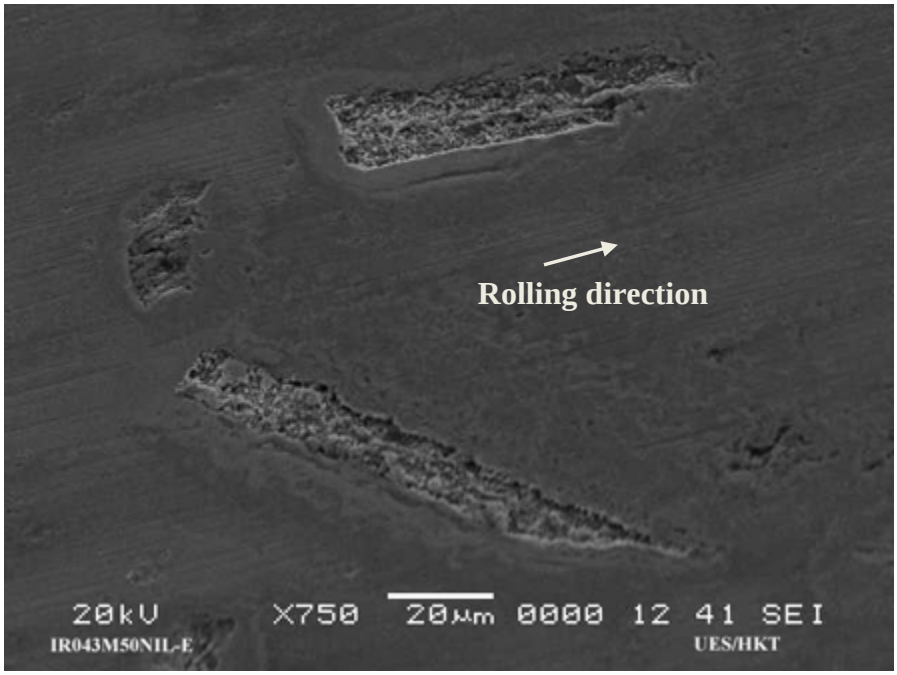

Figure 8. SEM showing surface damage on M50NiL inner raceway caused by hard TiN particles released from outer race cage-land surface coating.

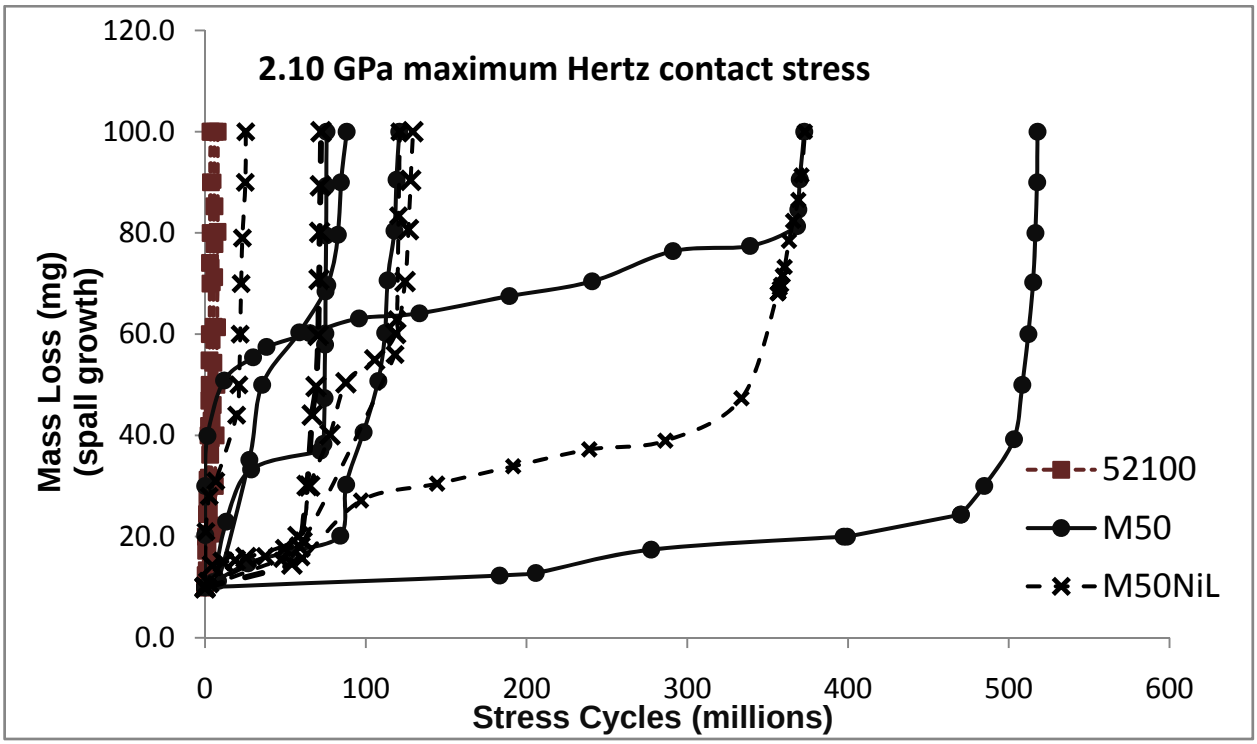

Figure 9. Spall propagation trend curves for new indented 52100, M50, and M50NiL at 2.10 GPa. Sample size, n = 5 for each material.

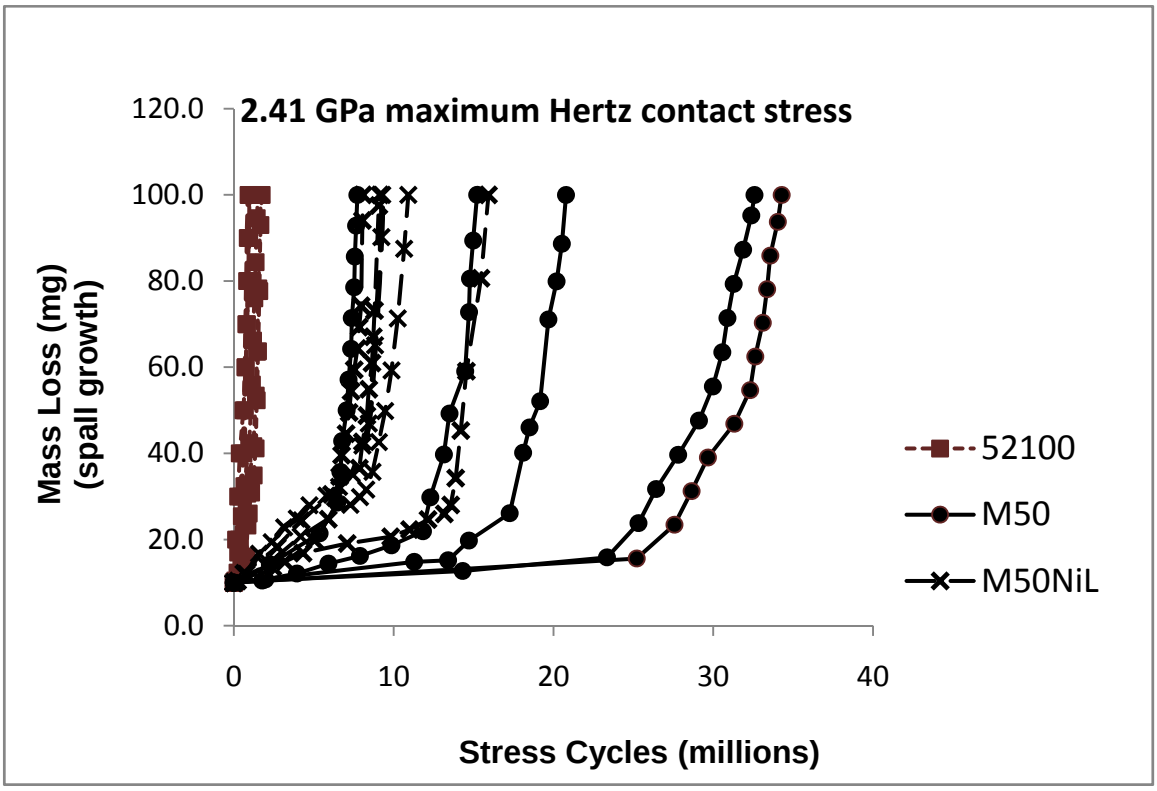

Figure 10. Spall propagation trend curves for new indented 52100, M50, and M50NiL at 2.41 GPa. Sample size, n = 5 for each material.

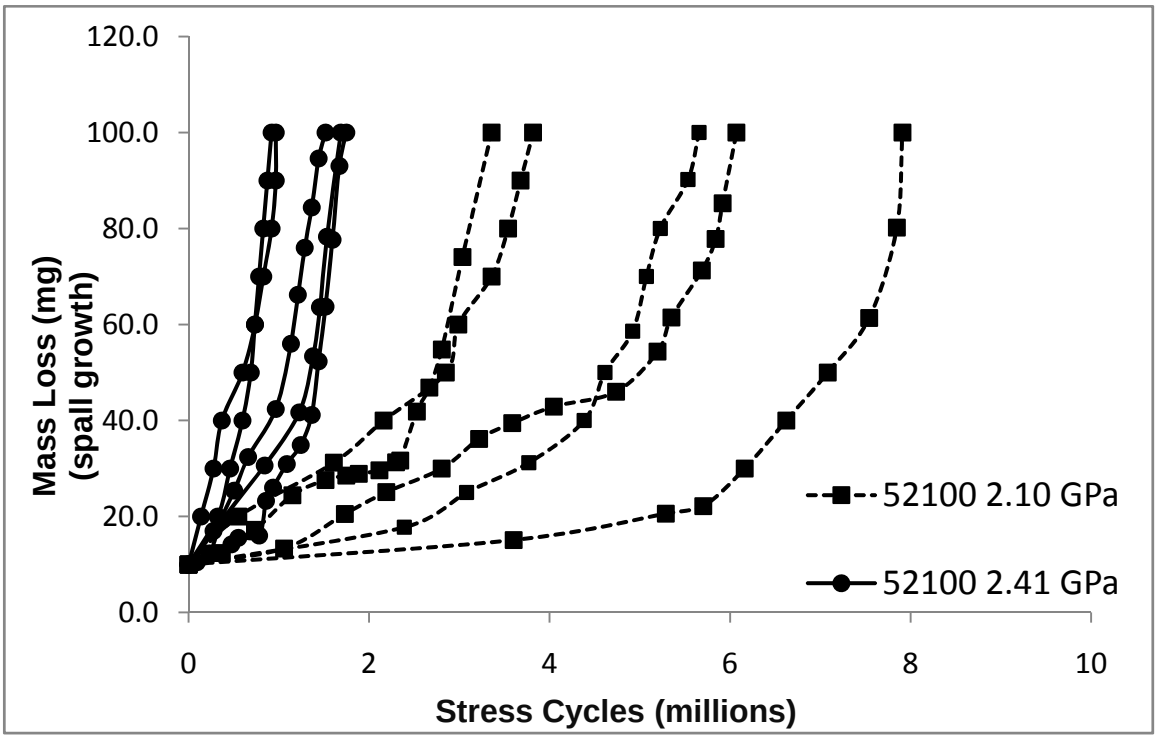

Figure 11. Effect of maximum Hertz contact stress on spall growth of new indented 52100 bearings.

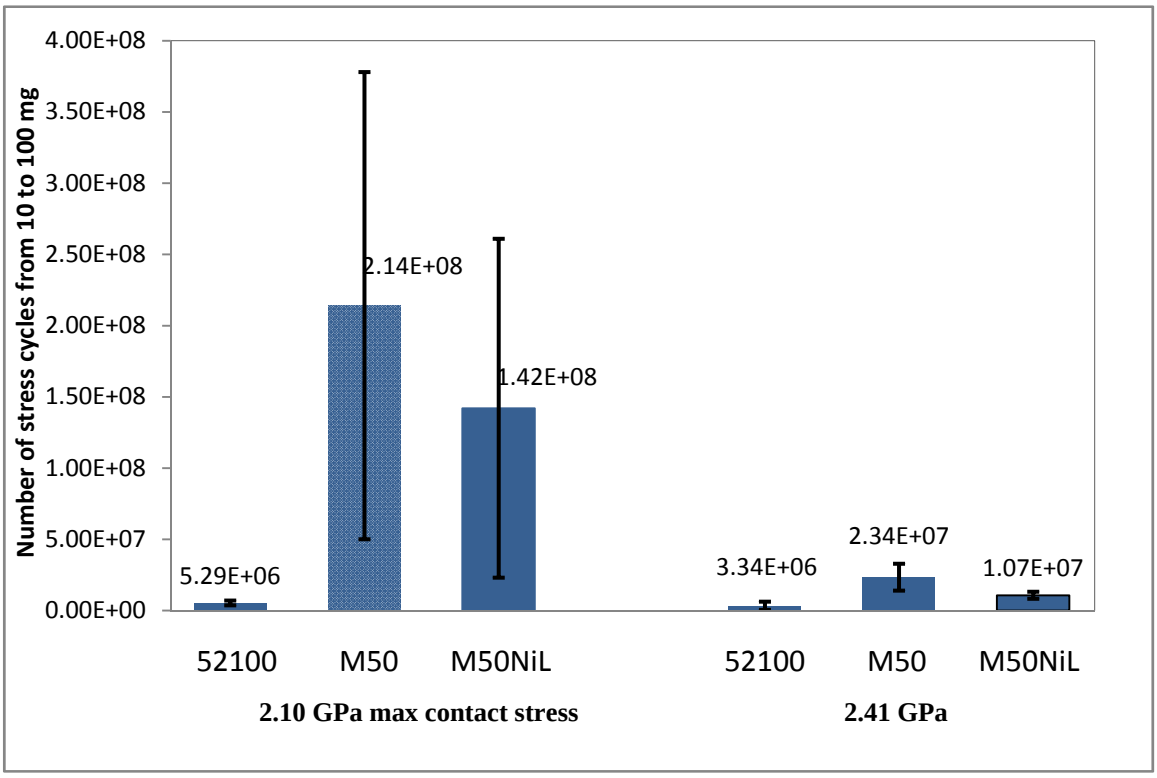

Figure 12. Effect of maximum Hertzian contact stress and material on spall propagation from 10 mg mass loss to 100 mg. New indented bearings with no prior accumulated stress cycles. Mean values and 95% confidence intervals shown, sample size n = 5.

(a) Spalled M50NiL inner raceway

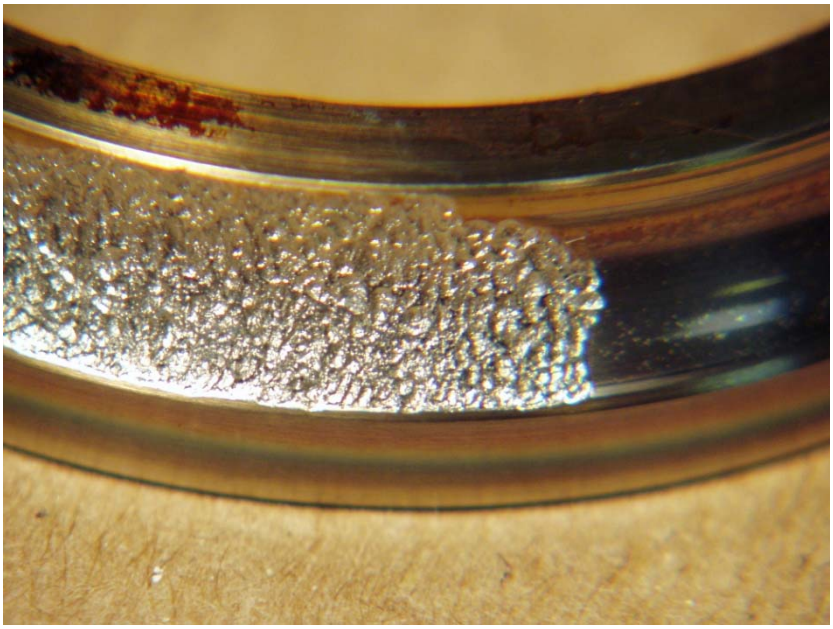

(b) Close up of spall front

Figure 13. Typical fatigue spalls after complete propagation (100 mg mass loss).

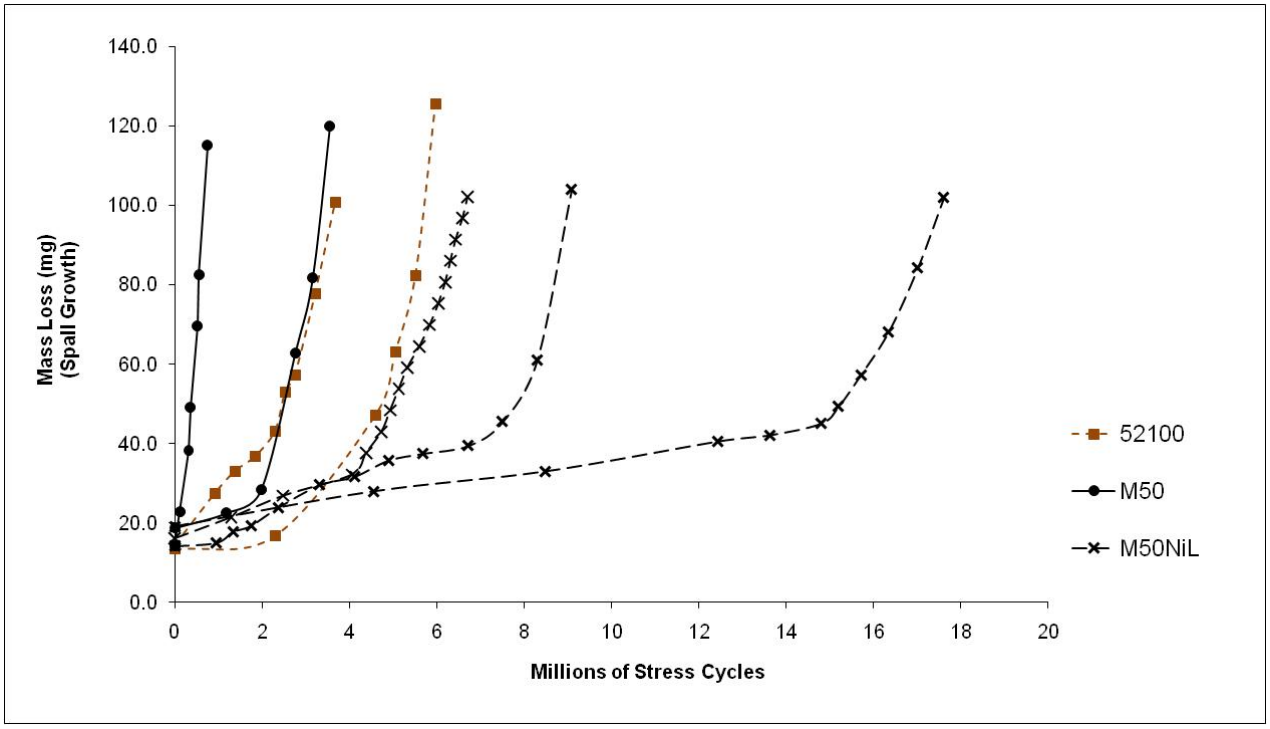

Figure 14. Spall propagation trend curves for bearings from life endurance tests. All at 2.41 GPa.

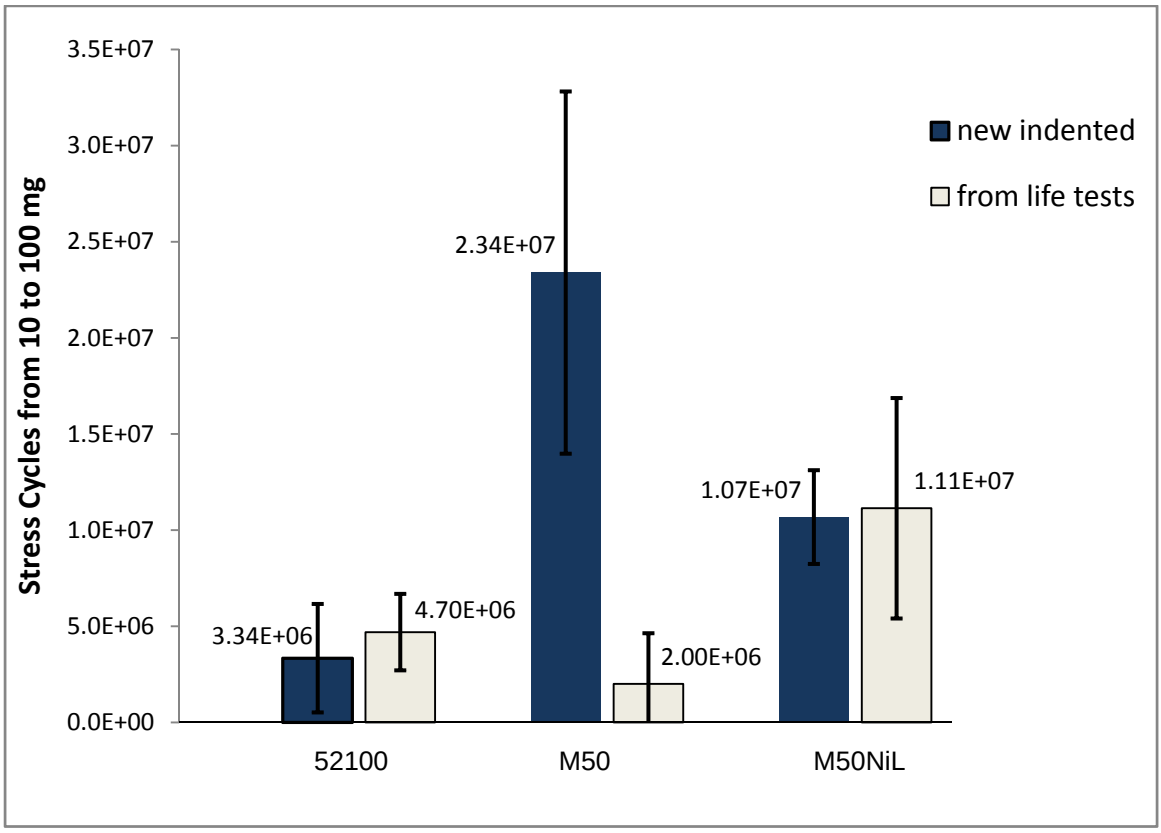

Figure 15. Spall propagation comparison between "new" indented bearings and bearings with accumulated stress cycles from life endurance tests. Mean number of stress cycles shown for spalls to propagate from 10 mg to 100 mg mass loss. All at 2.41 GPa, 95% confidence intervals shown.